Implicit Solvent Simulations of DNA and DNA−Protein Complexes: Agreement with Explicit Solvent vs Experiment

Jana Chocholoušová[†] and Michael Feig*[,†,‡]

Department of Biochemistry and Molecular Biology and Department of Chemistry, Michigan State University, East Lansing, Michigan 48824-1319

Received: May 5, 2006; In Final Form: July 3, 2006

Molecular dynamics simulations of biomolecules with implicit solvent reduce the computational cost and complexity of such simulations so that longer time scales and larger system sizes can be reached. While implicit solvent simulations of proteins have become well established, the success of implicit solvent in the simulation of nucleic acids has not been fully established to date. Results obtained in this study demonstrate that stable and efficient simulations of DNA and a protein−DNA complex can be achieved with an implicit solvent model based on continuum dielectric electrostatics. Differences in conformational sampling of DNA with two sets of atomic radii that are used to define the dielectric interface between the solute and the continuum dielectric model of the solvent are investigated. Results suggest that depending on the choice of atomic radii agreement is either closer to experimental data or to explicit solvent simulations. Furthermore, partial conformational transitions toward A-DNA conformations when salt is added within the implicit solvent framework are observed.

Introduction

Nucleic acids are essential biological molecules in all living organisms as their function revolves around storage and transmission of genetic information in replication, transcription, and translation. All of these processes involve interactions between nucleic acids and proteins. A recurring theme in this context is the recognition of a specific DNA sequence[1−3] especially during the regulation of gene expression. Nucleic acids have been studied extensively with many experimental methods, such as NMR spectroscopy,[4] X-ray diffraction,[5−7] infrared spectroscopy,[8−10] and fluorescence spectroscopy.[11,12] Insight into the structure and mechanisms of nucleic acids can also be reached by theoretical and computational means.[13−23] Computer simulations are an especially powerful tool for exploring the structure and dynamics of nucleic acids by themselves[17,24−26] and in interaction with solvent[20,27−34] and proteins.[35−39]

Computer simulations of biomolecules in general and nucleic acids in particular are commonly carried out in explicit solvent to reflect interactions with their biological environment.[13,16,40] An explicit solvent representation provides the most detailed description of the solvation forces acting on biomolecular solutes. However, because the number of solvent molecules must be large enough to provide at least several layers of solvation so that bulk solvent properties are reached at the edge of the simulated system,[41] and to eliminate possible artifacts when periodic boundary conditions[42,43] are used, the size of the entire simulation system can easily reach 10^4 atoms for a short DNA duplex and 10^5 atoms for protein−DNA complexes. As a consequence, such simulations are computationally very demanding.

The computational cost due to an explicit representation of solvent may be alleviated by applying an implicit formalism instead. A popular implicit solvent approach is to approximate the solvent through continuum electrostatics.[44,45] In such a model, energetic contributions arise from a high dielectric solvent environment capturing the effect of the polarization response by the solvent. Such a model is described by the Poisson or Poisson−Boltzmann (PB) equation. The latter is employed when salt effects are considered. Traditionally, the PB equation is solved numerically by time-consuming finite difference methods.[46−51] Although the direct application of PB solutions to molecular dynamics simulations of biomolecules is possible,[52−58] the generalized Born (GB) formalism is used more often as a computationally more efficient approximation to the PB method.[59−67] In the GB formalism, the electrostatic free energy is expressed as a sum of self-interactions and pairwise interactions of atomic charges as devised by Still et al.[64]

$$\Delta G^{\mathrm{elec}}_{\epsilon_p \rightarrow \epsilon_w} = -\frac{1}{2}\left(\frac{1}{\epsilon_p} - \frac{1}{\epsilon_w}\right)\sum_{ij}\frac{q_i q_j}{[r_{ij}^2 + \alpha_i\alpha_j \exp(-r_{ij}^2/F\alpha_i\alpha_j)]^{1/2}}$$

where q_i is the charge of atom i of the solute, r_{ij} is the distance between two atomic sites i and j, ϵ_p and ϵ_w are the interior and exterior solvent dielectric constant, and F is a constant usually set to 4 or 8.[60] The critical aspect of any GB method is the calculation of the Born radii, α_i.[68] According to the Coulomb field approximation,[69,70] Born radii can be calculated as

$$\frac{1}{\alpha_i} = \frac{1}{R_i} - \frac{1}{4\pi}\int_{\mathrm{solute}, r>R_i}\frac{1}{r^4}\,\mathrm{d}V$$

where R_i refers to the atomic van der Waals radius and the integration is performed over the entire solute cavity. This expression can be approximated by a discrete sum of overlap-

* Address correspondence to this author. Phone: (517)-432-7439. Fax: (517)-353-9334. E-mail: feig@msu.edu.
† Department of Biochemistry and Molecular Biology.
‡ Department of Chemistry.

10.1021/jp0627675 CCC: $33.50
Published on Web 08/05/2006

ping atomic values,[65,67,71,72] but more accurate methods calculate the integral numerically and also involve higher order terms.[60,62,73] The effective Born radius corresponds to the radius that would return the electrostatic energy of the system according to the Born equation if all other atoms in the molecule were uncharged. The Born radius can be interpreted roughly as the distance of a given atom from the solvent boundary.

The accuracy of a continuum dielectric model strongly depends on the exact definition of the solute−solvent boundary. This boundary may be defined approximately from an overlap of atomic van der Waals spheres.[74] An improved description is obtained with the so-called molecular surface,[75] where a probe radius representative of a solvent molecule is rolled around the van der Waals surface so that small, solvent-inaccessible crevices on the surface and cavities inside the solute are excluded. A similar effect can also be achieved by augmenting the atomic radii by a small amount.[55] The common choice of atomic van der Waals radii (as given by σ in molecular mechanics Lennard-Jones potentials) to define the size of the atomic spheres and consequently the dielectric boundary is a good first approximation of equilibrium contact distances in solute−solvent interactions. However, strong electrostatic interactions for example in salt bridges or solute−solvent hydrogen bonding interactions may result in substantially different equilibrium distances between interacting atoms. Therefore, modified sets of atomic radii have been developed.,[76−80] including a set of atomic radii for nucleic acids.[81] These radii were derived from an analysis of radial solvent charge densities obtained from explicit solvent molecular dynamics simulations and comparison with explicit solvent electrostatic solvation free energies.

The application of GB- or PB-type implicit solvent models has been successful in many simulations of proteins.[59,66,72,78,82−94] However, the application of implicit solvent methods and especially GB or PB continuum models to nucleic acids has been limited.[95−98] Successful molecular dynamics simulations of a DNA decamer with use of the generalized Born model have been described by Tsui and Case.[95] From these simulations substantial deviations from the starting structure (3.3 Å) after a relatively short simulation (2 ns) were reported. Because strong and specific interactions between nucleic acids and solvent are well documented,[20,29,30,32,99−103] it is not surprising that reliable stable simulations of nucleic acids were not successful until the Ewald[104] and particle mesh Ewald (PME)[105] methods or sufficiently large and smooth electrostatic cutoffs were applied to achieve an accurate treatment of long-range electrostatic interactions.[106,107] Therefore, it is not clear whether the application of continuum dielectric models to nucleic acids could be as successful as in protein systems without the addition of any explicit solvent.

Previous experimental,[108,109] theoretical,[110,111] and computational studies[31,112−114] have indicated that salt effects influence the structure and dynamics of nucleic acids. In particular, high salt concentrations appear to be related to a propensity toward A-DNA, at least in C/G base pairs.[115] While open questions remain with respect to the exact mode of ion interactions with A- or B-form DNA, it is also unclear whether the implicit inclusion of salt can lead to increasing conformational sampling of A-DNA features.

In this paper, DNA and protein−DNA simulations with the GBMV method,[60,73] with and without the inclusion of salt effects,[97] are presented. The results are compared with explicit solvent simulations and experimental data. As the DNA test case, the well-studied DNA duplex d(CGCGAATTCGCG)$_2$, commonly known as the Drew−Dickerson dodecamer,[116] is used, where experimental data[116,117] and results from simulations in explicit solvent [25,118] are available for comparison. The protein−DNA complex studied here is the GCC-box binding domain (GBD) in complex with the target DNA[119] that was chosen due to its convenient size and the availability of experimental data for comparison. In the following the simulation methods are described in more detail before results are presented and discussed.

Methods

The CHARMM27 force field was used for nucleic acids[120] and proteins.[121,122] The CMAP torsion correction for protein backbone was applied in the simulation of the protein−DNA complex.[122,123] The solvent effects were treated implicitly by the GBMV method[60,73] as implemented in CHARMM. The GBMV parameters (as defined in the original papers[60,73]) were set to the following values: $\beta = -12$, $S_0 = 0.65$,[124] $C_0 = -0.1$, and $C_1 = 0.9$. Two sets of radii were considered: radii taken from the CHARMM force field Lennard-Jones σ values (denoted in the following as "default radii") and a set developed by Banavali and Roux[81] (denoted as "BR radii"). Both sets of radii are shown in Table 1. The hydrophobic contribution to the solvation free energy was calculated based on the solvent-accessible surface area with a surface tension coefficient of 15 cal/mol/Å^2. The calculation of solvent-accessible surface areas is implemented within the GBMV module.[60] Integration over the solute volume in the calculation of Born radii was performed with $N_\phi = 5$ (see definition in GBMV paper[60,73]) and 29 radial integration points. Based on the linearized Debye−Hückel approximation, the GB formalism was extended to modulate dielectric screening as a function of ionic concentration according to a previously suggested formalism.[125] The salt concentration is introduced via the parameter κ, which is the inverse of the Debye length. Here, a value equal to 0.33 Å^{-1} was used, which approximates a 1 M ionic solution with monovalent ions.

Molecular dynamics with use of the GBMV implicit solvent model were started from initial coordinates for the Drew−Dickerson dodecamer according to PDB code 1GIP[126] and for the GCC-box binding domain in complex with DNA from PDB code 1GCC.[119] The N-terminus of the protein system was blocked by acetylation (ACE) while the C-terminus was capped with *N*-methylamide. A canonical A-form of the Drew−Dickerson dodecamer was built with the program X3DNA[127] and also used as a starting structure and for comparison. In all simulations, the initial structure was first minimized and then subjected to an equilibration phase where 50 ps were run at 100 K, followed by 50 ps at 200 K and 50 ps at 300 K. On the basis of the results from a previous study[124] the MD simulations were run with a 1 fs time step. Therefore, it was not necessary to apply holonomic constraints to any of the bond lengths. Langevin coupling with a friction coefficient of 50 ps^{-1} was applied to all non-hydrogen atoms.[128] The length of the production phase was 20 ns in all cases. Analysis of the simulations was performed during the last 15 ns allowing 5 ns for initial equilibration.

Simulations were carried out with the CHARMM program,[129] version c31b1, in combination with the MMTSB (Multiscale Modeling Tools for Structural Biology) Tool Set.[130] Root-mean-square deviations (RMSD) were evaluated with ptraj.[131] Ptraj was also used to determine the NOE distances and sugar puckers. Nucleic acid helical parameters were calculated with the program FREEHELIX98.[132]

TABLE 1: Comparison of the Values of Heavy Atom Atomic Radii (in Å) in the Default Radii Set (default) and in the Set by Banavali and Roux[81] (BR)'

	atom	default radii	BR radii
ADE	N9	1.85	2.13
	N7/N3	1.85	1.69
	N1	1.85	1.75
	N6	1.85	1.50
	C2	1.90	2.15
	C4/C5/C6	1.90	2.12
	C8	1.90	1.60
	H8/H2	1.10	1.50
	H61/H62	0.2245	1.50
GUA	N9	1.85	2.13
	N7/N3	1.85	1.69
	N1/N2	1.85	1.50
	O6	1.70	1.55
	C4/C5/C6	1.90	2.12
	C2	1.90	2.15
	C8	1.90	1.60
	H21/H22/H1	0.2245	1.50
	H8	1.10	1.50
CYT	N1	1.85	2.20
	N3	1.85	1.68
	N4	1.85	1.40
	O2	1.70	1.60
	C5/C6	1.90	1.50
	C2	1.90	2.04
	C4	1.90	2.12
	H5/H6	1.10	1.50
	H41/H42	0.2245	1.50
THY	N1	1.85	2.20
	N3	1.85	1.50
	O2/O4	1.70	1.60
	C4	1.90	2.12
	C5/C6	1.90	1.50
	C2	1.90	2.04
	C5M	2.04	1.50
	H3	0.2245	1.50
	H6	1.10	1.50
	H51/H52/H53	1.34	1.50
all	P	2.15	2.35
	O1P/O2P	1.70	1.49
	O5′/O3′	1.77	1.65
	O4′	1.77	1.55
	C2′	2.01	1.84
	C5′	2.01	1.71
	C1′	2.275	1.71
	C4′	2.275	1.64
	C3′	2.275	1.87
	H4′/H1′/H3′	1.32	1.50
	H5′/H5″/H2′/H2″	1.34	1.50

Results

Base Separation Energy Profiles. Energy profiles (internal energy + free energy of solvation) were calculated for the separation of initially hydrogen-bonded DNA nucleotides by translating one of the bases along the *x*-axis indicated in Figure 1. A comparison of the profiles calculated for the CHARMM default radii and the BR radii (see Figure 2) shows that the BR radii stabilize base pairing by 3−5 kcal/mol relative to the default CHARMM radii along the chosen separation coordinate. While the profiles highlight the differences with the two sets of atomic radii used in the continuum solvent model, it should be emphasized that the energy profiles are not meant to represent free energy profiles because conformational variation in degrees of freedom other than the *x*-coordinate are not sampled.

Simulations of DNA with the Default CHARMM Radii. Molecular dynamics simulations of the Drew−Dickerson dodecamer with the default set of radii implemented in CHARMM were carried out over 20 ns. The simulation was analyzed primarily through the calculation of root-mean-square deviations (RMSD) from the experimental structure and canonical A-DNA, sugar puckers, and helical parameters. The RMSD values with respect to the experimental structure (1GIP) and canonical A-form DNA are shown in Figure 3a. As can be seen, the DNA structure remained stable over the course of the entire simulation period. The conformations sampled during the simulations deviate somewhat further from the experimental structure during the first 10 ns, as far as 3.2 Å, but return closer to the experimental structure with RMSD values generally less

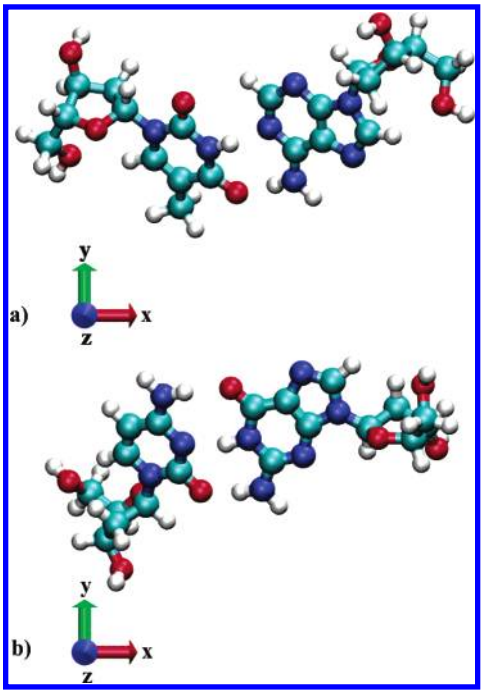

Figure 1. DNA base pairs in the coordinate system used for translation during the calculation of separation energy profiles.

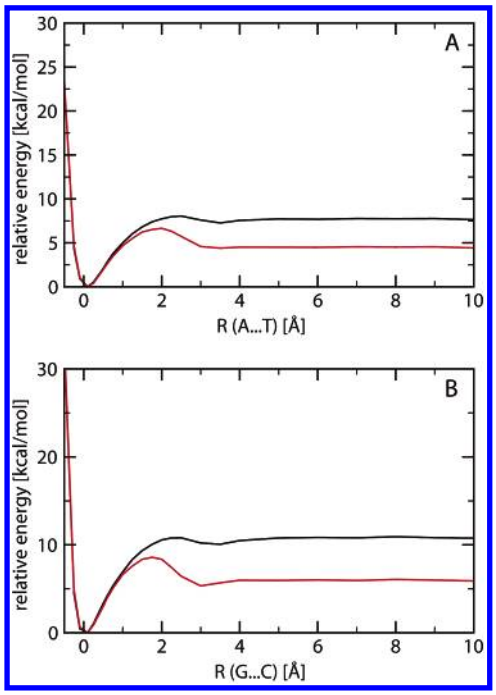

Figure 2. Dependence of the total energy (internal energy + free energy of solvation) on base pair separation *R* along the *x* axis (as defined in Figure 1) in (a) G...C and (b) A...T base pairs. Different sets of atomic radii (BR radii: black curve; default CHARMM radii: red curve) that were used in the definition of the implicit solvent dielectric interface are compared.

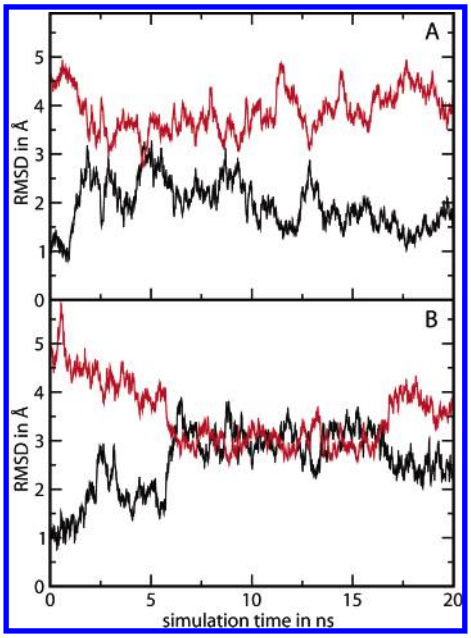

Figure 3. Heavy-atom RMSD in Å calculated with respect to the initial structure (black) and with respect to canonical A-form for the same sequence (red) from simulations with the default CHARMM radii: (a) no salt and (b) added salt. The terminal base pair were excluded in the RMSD calculation.

than 2 Å over the last 5 ns. The average RMSD over the last 15 ns of the simulation is found to be 1.9 ± 0.4 Å when compared to the experimental structure and 3.9 ± 0.4 Å when compared to canonical A-DNA. At all times but a very short interval around 5 ns the RMSD with respect to the canonical A-form is larger than the RMSD with respect to the experimental structure. The experimental structure and the final structure from the simulations are depicted in Figure 4, parts a and c, respectively. As can be seen, the structures are very similar. However, the simulated structure appears to be slightly bent with a compressed major groove and enlarged minor groove at the top end. Furthermore, one of the terminal bases opened up (around 10 ns) and is interacting with other base pairs.

Standard helical parameters are summarized in Table 2 along with reference data from a database survey of experimental structures in A- and B-form[118] and results from simulations of the same dodecamer in explicit solvent with the same force field.[118] The average parameters from the implicit solvent simulation are between A- and B-form values, but lie closer to B-DNA. They are in very good agreement with the average helical parameters from the explicit solvent simulations, albeit with standard deviations that are about twice as large as with explicit solvent suggesting a higher degree of fluctuations with implicit solvent.

An inspection of the ribose sugar pseudorotation angles provides another means of characterizing whether the DNA structure has adopted A- or B-form conformations. Individual time series of the pseudorotation angles for all 24 sugars are available as Supporting Information (Figure SF1). Percentages of simulation time spent either near the C2′-endo conformation (120 to 190°), indicative of B-DNA, or near C3′-endo (−10 to 60°), indicative of A-DNA, are given in Table 3. In agreement with the helical parameters, B-DNA are sampled most of the time, but A-DNA sugar conformations are found at a significant fraction of the time for some of the nucleotides, especially pyrimidines.

Simulations of DNA with the Set of Atomic Radii by Banavali and Roux. Molecular dynamics simulations of the Drew−Dickerson dodecamer performed with the atomic radii proposed by Banavali and Roux were also carried out over 20 ns simulation time. With the BR radii the DNA also remained stable in B-form as evidenced by the final structure shown in Figure 4e. Some bending of the helix at the top and minor base fraying at the bottom is apparent, but otherwise the final structure is remarkably close to the experimental structure. A closer look at the trajectory reveals that the RMSD from the experimental structure remains below 2 Å during nearly the entire trajectory with an average of 1.7 ± 0.4 Å (see Figure 5a). At the same time, the RMSD from canonical A-DNA is high throughout the simulation with an average of 4.1 ± 0.4 Å. This result is in contrast to the simulation with the default CHARMM radii where conformations intermediate between B- and A-DNA, but still closer to B-DNA, are sampled.

An inspection of helical parameters from the simulation with the BR radii (see Table 2) confirms that the sampled conformations resemble canonical B-DNA closely. The helical parameters

TABLE 2: Selected Helical Parameters Adopted from MacKerell et al.[118] ("explicit solvent" and NDB-A and NDB−B averages from database survey) and Calculated from the GBMV MD Simulations with FREEHELIX with the Default CHARMM Radii ("default"), Radii by Banavali and Roux ("BR")[a]

	explicit solvent	NDB-A	NDB-B	default	BR
rise	3.4 ± 0.4	2.8 ± 0.4	3.4 ± 0.5	3.2 ± 0.8	3.4 ± 0.6
inclination	8.7 ± 3.0	14.0 ± 4.9	2.8 ± 7.7	7.6 ± 9.2	5.8 ± 4.4
roll	5.6 ± 3.0	6.9 ± 4.7	1.9 ± 6.0	5.5 ± 7.2	2.3 ± 7.8
twist	34.9 ± 2.5	32.3 ± 3.8	35.7 ± 5.5	33.8 ± 5.9	35.6 ± 4.6
xdp	−0.9 ± 0.4	−4.1 ± 0.8	0.0 ± 1.4	−0.4 ± 1.5	−0.2 ± 0.8
propeller	−11.4 ± 5.4	−9.2 ± 6.3	−11.3 ± 8.2	−12.1 ± 9.3	−12.2 ± 8.4
slide	0.1 ± 0.3	−1.4 ± 0.4	0.4 ± 0.7	−0.2 ± 0.4	−0.1 ± 0.4

	Added Salt			
	default			
	1−6 ns	7−16 ns	16−20 ns	BR
rise	3.2 ± 0.6	3.0 ± 0.7	3.2± 0.6	3.4± 0.6
inclination	9.1 ± 9.8	18.9 ± 7.3	13.1± 7.6	1.7± 4.6
roll	5.3 ± 7.4	8.5 ± 7.3	6.9 ± 6.8	2.5 ± 7.4
twist	35.1 ± 4.9	35.6 ± 6.1	35.3 ± 5.8	35.9 ± 4.5
xdp	−1.2 ± 1.1	−2.1 ± 1.0	−1.6 ± 0.9	−0.1 ± 0.8
propeller	−12.5 ± 9.4	−11.9 ± 8.1	−12.0 ± 8.8	−12.7 ± 8.7
slide	−0.1 ± 0.5	0.1 ± 0.4	0.0 ± 0.5	0.0 ± 0.5

[a] Averages were calculated from all nonterminal bases or base pairs. Rise, *x*-displacement, and slide are given in Å. Inclination, roll, twist and propeller twist are given in deg.

TABLE 3: Percentage of Sampling Ribose Pseudorotation in the Intervals [120,190] (C2′-endo, B-DNA, first number) and [−10,60] (C3′-endo, A-DNA, second number) during the Last 15 ns of Simulations with Different Sets of Radii and with and without Salt

base	CHARMM radiino salt		CHARMM radii1 M salt		BR radiino salt		BR radii1 M salt	
strand 1								
C	27	61	39	41	54	18	52	27
G	92	4	96	0	97	0	70	28
C	30	58	92	1	69	23	26	68
G	95	0	95	0	94	1	95	1
A	97	0	54	43	99	0	98	0
A	98	0	98	0	96	0	95	0
T	27	49	23	36	86	3	88	4
T	78	18	47	50	93	0	82	11
C	73	22	90	6	45	50	31	66
G	89	5	96	0	98	0	98	0
C	60	25	63	30	69	27	97	0
G	93	1	91	1	93	2	94	0
strand 2								
C	51	19	48	33	51	16	40	42
G	93	2	94	0	96	1	36	62
C	53	28	91	2	52	37	19	80
G	94	0	93	0	97	0	97	0
A	95	3	98	0	91	7	96	0
A	97	0	0	99	97	0	97	0
T	44	27	0	100	89	0	88	4
T	60	35	98	0	96	0	96	1
C	30	66	85	11	14	84	48	49
G	33	64	95	0	98	0	69	29
C	98	0	98	0	94	1	57	41
G	88	0	87	1	90	4	94	1

averaged from the simulation are very similar to the averages from a NDB (Nucleic Acid Database[5]) survey of known B-DNA structures.[133] Only the inclination angle deviates somewhat more from canonical B-DNA values. Furthermore, in all cases except for the propeller twist the average helical parameters obtained with the BR radii are closer to the NDB B-DNA averages than the average parameters from the default CHARMM radii simulation.

Individual sugar pseudorotation angles are shown in the Supporting Information (Figure SF2). It is found that most of the time C2′-endo (B-DNA) sugar puckers are sampled, with some nucleotides spending a fraction of the time also in C3′-endo (A-DNA) conformations. Table 3 quantifies the percentages spent in either conformation for each base. It is interesting that significant sampling of C3′-endo sampling is limited only to cytosine nucleotides compared to substantial C3′-endo sampling in both thymine and cytosine nucleotides with the default radii.

Inclusion of Salt Effects. Another set of implicit solvent simulations with either default CHARMM or Roux−Banavali radii was carried out with modified dielectric screening to mimic salt effects as described in the Methods section.[97] Figures 3b and 5b show the RMSD values with respect to the experimental structure and canonical A-DNA as a function of simulation time for simulations with 1 M salt. Final structures at the end of the simulations are shown in Figure 4d,f. The results suggest that conformations halfway between A- and B-form are sampled with the default CHARMM radii. At the beginning and end of the 20 ns simulation the structure is somewhat closer to the experimental B-form, but between 7 and 16 ns the sampled structure is equally far (3 Å) from either A- or B-DNA. In the simulation with the BR radii the DNA remains as close to B-DNA very similar to the simulation without added salt effects (1.7 Å) and equally far from A-DNA (5 Å).

The helical parameters calculated from both simulations confirm that the DNA structure in the simulation with the BR radii and added salt is very close to average B-DNA. In fact, because the inclination angle is in better agreement with the expected value for B-DNA it appears that the sampled conformations may be even closer to B-DNA than without addition of salt. In contrast, the structures sampled with the default CHARMM radii and added salt clearly sample A-like helical parameters, especially from 7 to 16 ns, although not all parameters, such as twist, display typical A-like values.

An analysis of the sugar puckers (details are shown in Figures SF3 and SF4, percentages are given in Table 2) shows very similar sampling of C2′-endo and C3′-endo conformations with and without salt when the CHARMM radii are used. However, it appears that most cytosine and guanine base pairs sample C3′-endo conformations for a significantly larger part of the time when salt effects are added and the BR radii are employed.

Simulations Starting from Canonical A-Form. As a further test of the implicit solvent methodology, simulations of the Drew−Dickerson sequence were also started from canonical A-form in order to examine whether a transition to the experimental B-form can be observed. In both cases, the structures quickly moved from the A-form toward the B-form as can be seen from the RMSD plots in Figure 6. The structures at both simulations after 20 ns are clearly B-like (see parts g and h of Figure 4 in comparison with part b). It appears, though, that convergence to a similar structure with either starting conformation is only achieved with the CHARMM radii within the 20 ns simulation time, while the final structure with the BR radii in the simulation started from A-DNA is substantially different from the B-DNA conformations observed in the simulation started from the crystal structure.

The transition from A-DNA to B-DNA is accompanied by a sequential transition of sugar puckers from C3′-endo to C2′-endo starting from the terminal base pairs (see Figures SF5 and SF6). With the CHARMM default radii all but 8 bases have switched to C2′-endo after 20 ns, while with the BR radii 11 bases remain in C3′-endo suggesting that the transition is not complete even after 20 ns simulation time.

Simulation of the GCC-Box Binding Domain (GBD). The GBD with its target DNA was simulated for 10 ns with use of the GBMV method. Figure 7 shows the RMSD vs time for the

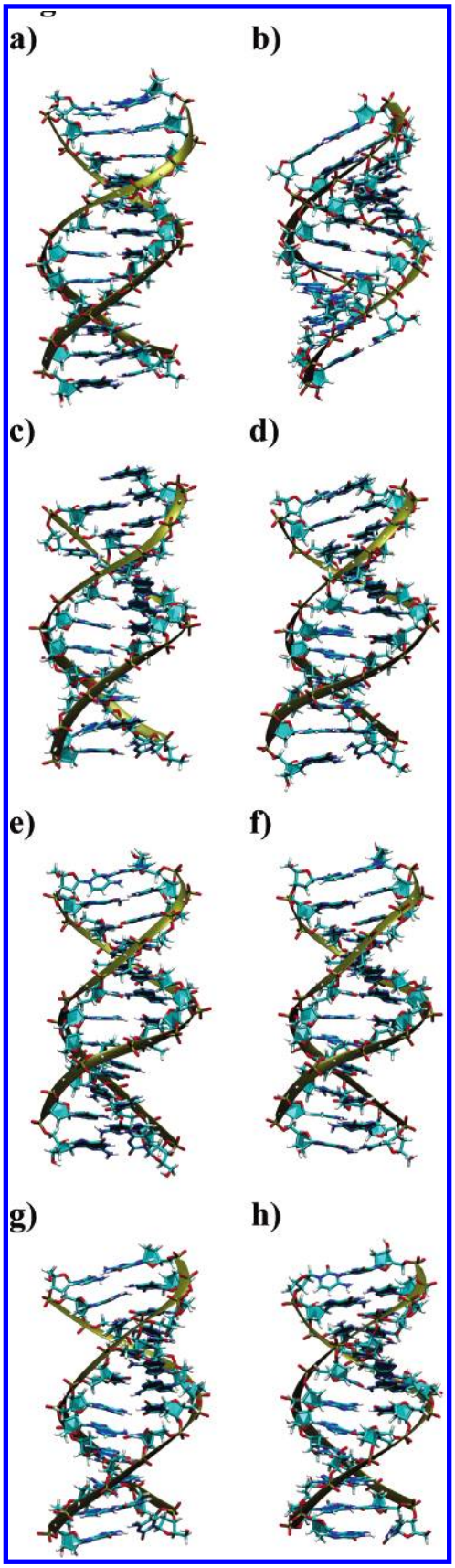

Figure 4. Structures of the Drew−Dickerson dodecamer: (a) experimental B-DNA, (b) canonical A-DNA structure; simulated structures (after 20 ns) with (c) default CHARMM radii, (d) default CHARMM radii and added salt, (e) BR radii, (f) BR radii and added salt, (g) default CHARMM radii started from A-DNA, and (h) BR radii started from A-DNA.

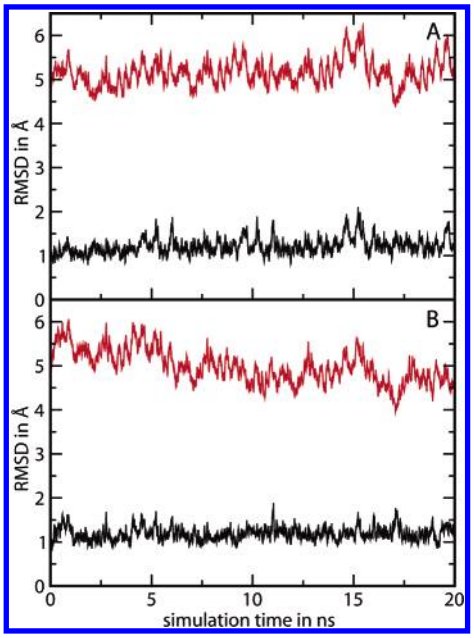

Figure 5. Heavy-atom RMSD in Å calculated with respect to the initial structure for simulations with the BR radii: (a) no salt and (b) added salt. Deviations from B-DNA are shown in black and from A-DNA in red. The terminal base pair were excluded.

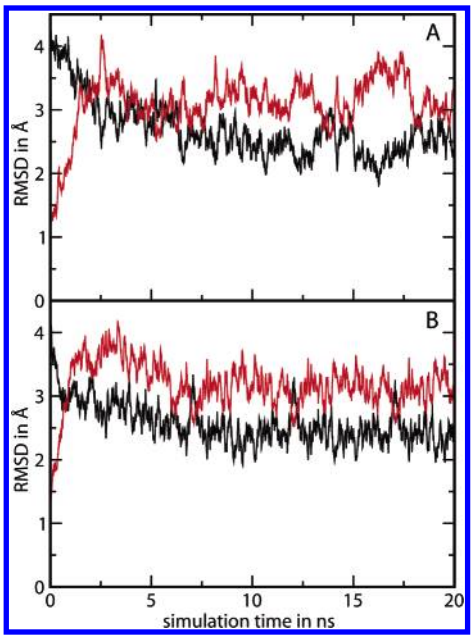

Figure 6. Heavy-atom RMSD in Å calculated from simulations where the initial structure was the canonical A-form of the Drew−Dickerson dodecamer: (a) default CHARMM radii (b) BR radii. RMSD with respect to the canonical A-form (red line) and with respect to the experimental structure (black line).

protein−DNA complex as well as for the protein and DNA separately. It is found that while the DNA remains highly stable (1.6 Å average after 4 ns) the protein varies more than 3 ns toward the end of the 10 ns simulation. Figure 8 illustrates how the initial (experimental) and final (simulated) structures compare. It can be seen that overall the integrity of the complex is maintained, while the largest changes are found for the protein residues near the termini.

The orientation of the protein surface with respect to the DNA has been measured experimentally by NMR spectroscopy.[119] The resulting NOE-derived distance restraints were monitored throughout the simulation to test the ability of the implicit

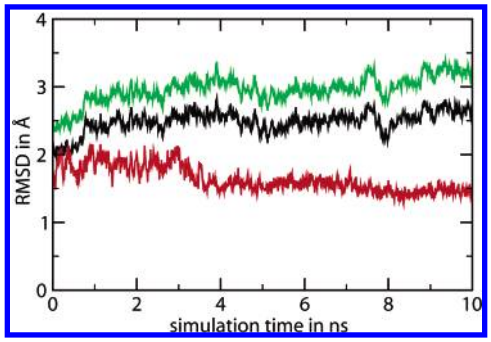

Figure 7. Heavy-atom RMSD calculated for different components of the GCC box binding domain with its target DNA: entire protein−DNA complex (black line), DNA only (red line), and protein only (green line).

solvent method to provide a realistic description of the protein−DNA interface. Table 4 shows NOE-derived restraints along with average atom−atom distances from the simulation and found in the reported experimental structure. The data show that the NOE restraints are violated in 2 cases out of 37 in both the experimental structure and the simulations. In 5 other cases the restraints are also violated in the simulation, however, only by small amounts. This finding indicates that the protein−DNA interface may be slightly distorted with respect to the experimental data, but is still overall well preserved.

Timing. The performance of nucleic acid simulations with GBMV was compared to explicit solvent simulations by measuring execution times for carrying out 100 steps of molecular dynamics on a 2.8 GHz Pentium IV CPU. The test system chosen is the Dickerson dodecamer described in this study with the GBMV parameters described in the Methods section. For the explicit solvent simulations the DNA was solvated in a cubic box with a 10 Å water shell in each dimension resulting in a box size of 61.3 Å. The simulations were carried out with Particle-Mesh Ewald, using a 10 Å cutoff of the direct sum. The measured times are 24s/100 steps with GBMV and 92s/100 steps with explicit solvent. If one takes into account that the GBMV simulations should use a 1−1.5 fs time step[124] while the explicit solvent simulations can use a 2 fs integration time step, the GBMV simulations are about 2 to 3 times faster than the corresponding explicit solvent simulations.

TABLE 4: Intermolecular NOE Distance Restraints (in Å)[a]

	NOE connectivities			
DNA	protein	upper boundary	av/st dev	exptl
T3,H2′	Trp154,Hϵ1	6.0	3.4 ± 0.6	2.6
T3, H2′	Trp154,Hζ2	5.0	3.9 ± 1.0	2.9
T3,H2″	Trp154,Hζ2	5.0	3.9 ± 0.7	3.8
T3,H6	Trp154,Hζ2	6.0	4.9 ± 0.6	4.8
T3,H5	Trp154,Hζ3	6.0	4.3 ± 1.0	3.0
A4,H8	Trp154,Hζ2	3.5	3.2 ± 0.7	2.6
A4,H2′	Trp172,Hϵ1	6.0	3.0 ± 0.5	3.4
A4,H2′	Trp172,Hζ2	6.0	3.3 ± 0.7	3.0
A4,H3′	Thr175,Hβ	5.0	4.4 ± 1.4	3.6
A4,H3′	Thr175,Hγ2	6.0	4.7 ± 1.3	2.8
G5,H2″	Trp172,Hδ1	6.0	3.0 ± 0.4	2.1
G5,H3′	Trp172,Hϵ1	5.0	4.0 ± 0.4	4.1
G5,H8	Trp172,Hϵ1	5.0	3.1 ± 0.4	3.6
G5,H8	Trp172,Hζ2	5.0	3.4 ± 0.7	3.9
G5,H8	Trp172,Hη2	5.0	5.0 ± 0.9	2.4
C6,H4**	Trp172,Hζ3	6.0	3.7 ± 0.8	3.4
C6,H4*	Trp172,Hη2	5.0	3.7 ± 0.7	4.0
C6,H5	Trp172,Hϵ3	5.0	3.4 ± 0.5	3.8
C6,H5	Trp172,Hζ3	5.0	3.7 ± 0.7	3.2
C6,H5	Trp172,Hη2	6.0	***6.3*** ± 0.8	2.7
C6,H6	Trp172,Hβ2	6.0	4.2 ± 0.5	5.7
T16,H2″	Arg162,Hϵ	6.0	4.4 ± 0.4	3.2
T16,H3′	Arg162,Hϵ	6.0	***6.1*** ± 0.4	5.4
T16,H3′	Arg162,Hδ#	6.0	3.6 ± 0.4	4.2
T16,H6	Arg162,Hϵ	6.0	4.2 ± 0.5	3.4
T16,H6	Arg162,Hδ#	3.5	3.0 ± 0.3	2.1
T16,H5	Arg162,Hϵ	5.0	4.0 ± 0.8	4.7
T16,H5′	Arg162,Hδ#	6.0	4.7 ± 0.8	4.1
G17,H8	Arg162,Hβ#	6.0	3.9 ± 0.4	3.2
G17,H8	Arg162,Hϵ	6.0	***7.1*** ± 0.5	3.3
C19,H5	Arg150,Hγ#	6.0	4.2 ± 0.6	3.2
C19,H5	Arg150,Hδ#	5.0	2.4 ± 0.3	2.5
C19,H6	Arg150,Hδ#	3.5	***3.6*** ± 0.9	***4.7***
C22,H4**	Trp154,Hζ2	6.0	***7.3*** ± 1.3	***6.4***
C22,H4*	Trp154,Hζ2	5.0	***5.1*** ± 1.2	4.1
C22,H4**	Trp154,Hη2	6.0	***6.7*** ± 1.2	5.7
C22,H4*	Trp154,Hη2	6.0	4.8 ± 1.0	3.6

[a] The third column shows the upper boundaries, the fourth column contains the average values (in Å) ± the standard deviations calculated from the GBMV simulation, the last column shows the values measured from the initial structure. Proton (in C6 and C22) binding to the partner base is labeled *, while the other is labeled **. The symbol # means that the proton of the methylene group is not identified uniquely. Violations are indicated in bold italics.

Discussion

Simulations of biomolecules generally aim at providing the most realistic description of molecular structure and dynamics within the limits of computer resources. Classical all-atom models of biomolecules with an explicit solvent environment are generally believed to provide the best compromise between accuracy and affordability for the study of many biological questions at the current time. The replacement of explicit solvent with an implicit solvent representation offers computational advantages, but the extent to which such an approximation of

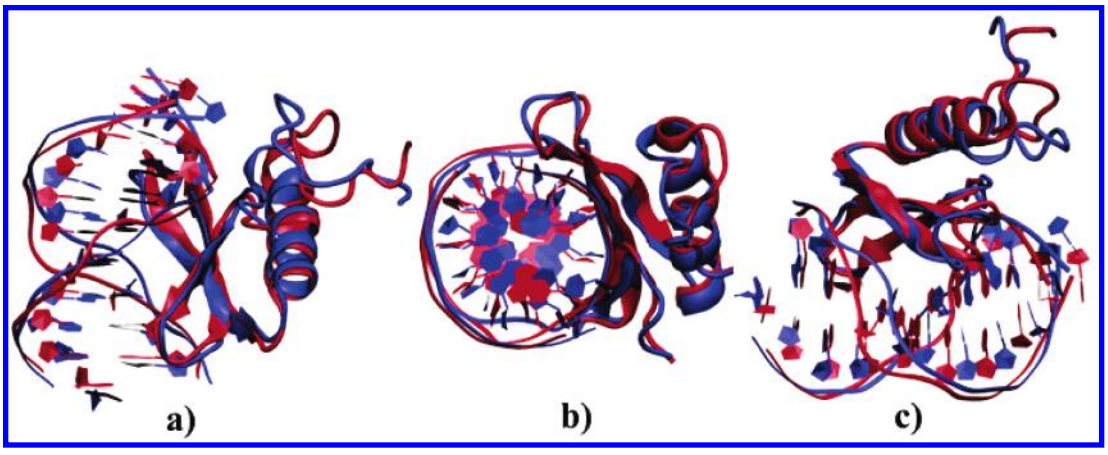

Figure 8. GCC box binding domain with its target DNA. Superposition of the initial (red) and the final (blue) structures.

the undoubtedly important interactions with the environment affects conformational sampling of biomolecules remains unclear.

The results presented here address the question of how well nucleic acids can be sampled with a generalized Born-type implicit solvent model. A previous simulation of DNA with a generalized Born model was moderately successful.[95] The simulations shown here with the GBMV model are much longer with the DNA structure remaining very close either to the experimental structure (BR radii) or to results from explicit solvent simulations (default CHARMM radii). There are three major findings to be reported from this study:

First, it is possible to obtain very stable simulations of nucleic acids with a two-dielectric continuum implicit solvent description. Such a result is somewhat unexpected because first solvation shell water molecules near DNA are known to have structural and dynamic properties that are very different from bulk solvent.[20,29,32,103,117,134] Because even 20 ns simulations are still relatively short compared to the time scales on which conformational changes in biomolecules may occur, the possibility exists that the observed conformations are only representative of a meta-stable minimum. To address this issue, simulations were also started from A-DNA with the expectation that the conformations revert back to the experimental structure. With both sets of radii the structures indeed approach B-DNA conformations fairly rapidly. The transition is nearly complete after 20 ns simulation time with the default CHARMM radii and partially complete with the BR radii. These findings suggest that the lowest energy conformations sampled with implicit solvent are in fact the B-DNA structures close to the experimental structure. Another concern is that a relatively high value for the friction coefficient may lead to artificial stabilization of a given structure.[59] In the simulations discussed here we used a friction coefficient of 50 ps^{-1} as suggested by Pastor et al.,[128] but we also tested a lower value of 5 ps^{-1} with the CHARMM radii. While detailed results are not shown here, the DNA also remained stable and close to B-form DNA over 10 ns with a friction coefficient of 5 ps^{-1}. In fact, it is found that the structures remain slightly closer to the experimental structure with the lower friction coefficient than with the larger value. While the best choice of the friction coefficient in Langevin simulations for obtaining valid kinetic information with implicit solvent simulations is still an unresolved question, it appears that the conformational sampling of DNA discussed here is largely unaffected by different choices of the friction coefficient.

In the simulation with the default CHARMM radii and no added salt the terminal base pair was found to open up and interact with other base pairs in a triplet-like arrangement. Similar end effects are also commonly observed in explicit solvent simulations of short DNA sequences.[135−139] To test whether terminal base pair opening is a more common feature of simulations under these conditions (default CHARMM radii and no added salt) a second simulation with a different random seed but otherwise identical conditions was carried out (data not shown). In that simulation, similar base pair opening and interaction with other base pairs was also observed after a few nanoseconds. Although B-DNA geometries were maintained this finding would suggest that with implicit solvent and default CHARMM radii base pair hydrogen bonding and/or base stacking interactions may be slightly underestimated. In the simulations with the BR radii that stabilize base pair hydrogen bonding compared to the default CHARMM radii (see Figure 1) terminal base pair opening was not observed.

Second, the inclusion of salt in the implicit solvent framework does appear to induce the sampling of more A-like conformations. With the default CHARMM radii the overall structure clearly resembled A-DNA more closely when salt was included compared to the simulation without salt. With the BR radii, more extensive sampling of C3′-endo sugar puckers, indicative of A-DNA, was observed when salt was included. It is remarkable, however, that the sampling of C3′-endo conformations did not increase substantially with salt and the default CHARMM radii, while the overall structure remained very clearly B-form with the BR radii despite sampling of C3′-endo sugar puckers for significant parts of time in the C/G base pairs. Experimental evidence does not indicate that the Drew−Dickerson dodecamer would in fact undergo a transition to full A-form DNA under high salt conditions. Typically, A-form DNA is only observed at high salt and in low dielectric solvent for sequences with a high content of C/G base pairs.[140−143] Therefore, it appears that the results with the BR radii are in better agreement with experiment since the overall structure remains close to B-form, while only the sugar puckers of cytosine/guanine base pairs display a tendency toward A-form conformations. The effect on conformational sampling of a more substantial change toward an A-form structure at high salt with the CHARMM radii may be realistic for other sequences, but not for the Drew−Dickerson dodecamer.

While further tests are needed to evaluate the ability of implicit solvent models with added salt to fully reproduce experimental data, the success of such an approach is limited not just by the lack of specific solvent interactions but also by the underlying Debye−Hückel theory[144,145] that is only a good approximation for very dilute solutions. Previous studies have commented on reasonable accord between PB and GB models up to 1 M added salt;[125] however, the effects of higher salt concentrations cannot be expected to be reasonably captured with the approach followed here. This is a serious limitation given that DNA conformation responds to salt concentrations of about 1 M and higher.

Third, the choice of atomic radii that define the dielectric boundary in the implicit solvent model significantly affects the conformational sampling of DNA. The simulations presented here suggest an intriguing result: With the default CHARMM radii previous explicit solvent simulations are matched closely;[118] however, when the BR radii derived from radial distribution functions and matched to explicit solvent free energies are applied, the agreement with respect to the experimental data becomes even better than that with the explicit solvent simulations. This raises the issue whether implicit solvent models should be optimized to fit explicit solvent models (which they approximate) or experimental data (which they ultimately seek to reproduce closely). An optimization with respect to experiment while ignoring data from explicit solvent simulations essentially introduces an additional empirical component into an energetic description that is otherwise mostly based on physical principles. Empirical force field components present the danger of poor transferability, but the more fundamental question is why an implicit solvent model may be able to provide better agreement with experiment than the more detailed explicit solvent description. Explicit solvent clearly has an advantage in providing specific solute−solvent interactions in the first solvation shell and it is difficult to imagine how an implicit description could be advantageous in this regard. However, solvent models commonly in use do not account for electronic polarizability, while implicit solvent models do so in an implicit fashion. A recent comparison of DNA simulations with polariz-

able and nonpolarizable force fields suggests that the inclusion of polarization effects does in fact improve the quality of the simulation with less deviation from the experimental structure.[146] Although in this study both the solvent and the nucleic acid were polarizable, it supports the idea that implicit solvent may improve the quality of nucleic acid simulations by capturing solvent polarizabilities more effectively. Without understanding this issue better, the question of which set of radii should be used in applications remains unclear: The default CHARMM radii appear to provide a close approximation of the explicit solvent model. However, the BR radii seem to be the better choice if the goal is to match experimental data.

Further application of the implicit solvent model to a protein−DNA complex, the GCC box binding domain with its target DNA, was also successful. Essentially, both the nucleic acid and protein remain very stable over the course of the simulation. The largest deviations were found at the termini of the protein where larger conformational flexibility is expected from the NMR data as well.[119] On the other hand, the protein−DNA interface is well maintained as evidenced by the agreement of simulated atom−atom distances at the interface with experimental NOE distance restraints. Again, it is somewhat surprising that a purely implicit solvent is able to preserve a protein−DNA complex close to the experimental structure without the addition of explicit solvent molecules at least near the protein−DNA interface. The slight violation of some of the NOE restraints suggests, however, that it may be possible to improve the quality of the simulations, for example by including selected explicit water molecules at the interface.

Finally, it should be stressed that in the present study only one DNA sequence and one protein−DNA complex are considered. Further studies on different systems and over longer simulation times will be needed to improve the statistics and confirm that the conclusions remain valid beyond the limited scope of the results presented here.

Conclusions

The results presented here demonstrate that stable simulations of DNA as well as a protein−DNA complex can be obtained by using an implicit solvent model with the GBMV generalized Born method. Depending on the choice of atomic radii that are used to define the dielectric interface between the solute and the continuum dielectric model of the solvent it is possible to either match closely conformational sampling from explicit solvent simulations (default CHARMM radii) or experimental data (BR radii). Furthermore, the inclusion of salt effects in the implicit model is found to lead to more extensive sampling of A-DNA features compared to simulations without added salt as would be expected from experimental data. The findings from this study suggest that implicit solvent models can be used to simulate nucleic acids and protein−nucleic acid complexes in a realistic fashion thus opening the door to longer simulation time scales and allowing the study of larger biomolecular complexes in future applications.

Acknowledgment. This work has been supported by NSF CAREER grant 0447799 and an Alfred P. Sloan Research Fellowship to M.F.

Supporting Information Available: Graphs of ribose pseudorotation angles as a function of time. This material is available free of charge via the Internet at http://pubs.acs.org.

References and Notes

(1) Garvie, C. W.; Wolberger, C. Recognition of specific DNA sequences. *Molecular Cell* **2001**, *8* (5), 937−946.

(2) Schwabe, J. W. R. The role of water in protein DNA interactions. *Curr. Opin. Struct. Biol.* **1997**, *7* (1), 126−134.

(3) Janin, J. Wet and dry interfaces: the role of solvent in protein−protein and protein−DNA recognition. *Struct. Folding Design* **1999**, *7* (12), R277−R279.

(4) Lane, A. N. Nmr-Studies of Dynamics in Nucleic-Acids. *Prog. Nucl. Magn. Reson. Spectrosc.* **1993**, *25*, 481−505.

(5) Berman, H. M.; Olson, W. K.; Beveridge, D. L.; Westbrook, J.; Gelbin, A.; Demeny, T.; Hsieh, S. H.; Srinivasan, A. R.; Schneider, B. The Nucleic-Acid Database−A Comprehensive Relational Database of 3-Dimensional Structures of Nucleic-Acids. *Biophys. J.* **1992**, *63* (3), 751−759.

(6) Hays, F. A.; Teegarden, A.; Jones, Z. J. R.; Harms, M.; Raup, D.; Watson, J.; Cavaliere, E.; Ho, P. S. How sequence defines structure: A crystallographic map of DNA structure and conformation. *Proc. Natl. Acad. Sci. U.S.A.* **2005**, *102* (20), 7157−7162.

(7) Williams, L. D. Between objectivity and whim: Nucleic acid structural biology. *DNA Binders Relat. Subjects* **2005**, *253*, 77−88.

(8) Guzman, M. R.; Liquier, J.; Taillandier, E. Hydration and conformational transitions in DNA, RNA, and mixed DNA-RNA triplexes studied by gravimetry and FTIR spectroscopy. *J. Biomol. Struct. Dyn.* **2005**, *23* (3), 331−339.

(9) Andrushenko, V. V.; Kornilova, S. V.; Lapinos, L. E.; Hackl, E. V.; Galkin, V. L.; Grigoriev, D. N.; Blagoi, Y. P. IR-spectroscopic Studies of Divalent Metal Ion Effects on DNA Hydration. *J. Mol. Struct.* **1997**, *408/409*, 225−228.

(10) Benevides, J. M.; Wang, A. H.-J.; Rich, A.; Kyogoku, Y.; Marel, G. A. van d.; Boom, J. H. v.; Thomas, G. J. The Raman Spectra of Single Crystals of r(GCG)d(CGC) and d(CCCCGGGG) as Model for A-DNA, their Structure Transitions in Aqueous Solution and Comparison with Double Helical Poly(dG)·Poly(dC). *Biochemistry* **1986**, *25*, 41−50.

(11) Barkley, M. D.; Zimm, B. H. Theory of Twisting and Bending of Chain Macromolecules; Analysis of the Fluorescence Depolarization of DNA. *J. Chem. Phys.* **1979**, *70*, 2991−3007.

(12) Häupl, T. Picosecond Fluorescence of Nucleic Acid Bases. *Chem. Phys. Lett.* **1997**, *280*, 520−524.

(13) Cheatham, T. E.; Kollman, P. A. Molecular dynamics simulations of nucleic acids. *Annu. Rev. Phys. Chem.* **2000**, *51*, 435−471.

(14) Kollman, P. A.; Massova, I.; Reyes, C.; Kuhn, B.; Huo, S.; Chong, L.; Lee, M.; Lee, T.; Duan, Y.; Wang, W.; Donini, O.; Cieplak, P.; Srinivasan, J.; Case, D. A.; Cheatham, T. E., III Calculating structures and free energies of complex molecules: combining molecular mechanics and continuum models. *Acc. Chem. Res.* **2000**, *33*, 889−897.

(15) Cheatham, T. E. Simulation and modeling of nucleic acid structure, dynamics and interactions. *Curr. Opin. Struct. Biol.* **2004**, *14* (3), 360−367.

(16) Giudice, E.; Lavery, R. Simulations of nucleic acids and their complexes. *Acc. Chem. Res.* **2002**, *35* (6), 350−357.

(17) Beveridge, D. L.; Young, M. A.; Sprous, D. Modeling of DNA via Molecular Dynamics Simulation: Structure, Bending, and Conformational Transitions. In *Molecular Modeling of Nucleic Acids*; Leontis, N. B., Ed.; American Chemical Society: Washington, DC, 1997; pp 260−284.

(18) Feig, M.; Pettitt, B. M. Experiment vs Force fields: DNA Conformation from Molecular Dynamics Simulations. *J. Phys. Chem. B* **1997**, *101*, 7361−7363.

(19) Feig, M.; Pettitt, B. M. Structural Equilibrium of DNA Represented with Different Force Fields. *Biophys. J.* **1998**, *75*, 134−149.

(20) Feig, M.; Pettitt, B. M. A Molecular Simulation Picture of DNA Hydration Around A- and B-DNA. *Biopolymers* (*Nucleic Acid Sci.*) **1998**, *48*, 199−209.

(21) Norberg, J.; Nilsson, L. NMR Relaxation Times, Dynamics, and Hydration of a Nucleic Acid Fragment from Molecular Dynamics Simulations. *J. Phys. Chem.* **1995**, *99*, 14876−14884.

(22) MacKerell, A. D., Jr.; Wiorkiewicz-Juczera, J.; Karplus, M. An All-Atom Empirical Energy Function for the Simulation of Nucleic Acids. *J. Am. Chem. Soc.* **1995**, *117*, 11946−11975.

(23) Banavali, N. K.; MacKerell, A. D. Free energy and structural pathways of base flipping in a DNA GCGC containing sequence. *J. Mol. Biol.* **2002**, *319*, 141−160.

(24) McConell, K. J.; Nirmala, R.; Young, M. A.; Ravishanker, G.; Beveridge, D. L. A Nanosecond Molecular Dynamics Trajectory for a B-DNA Double Helix: Evidence for Substates. *J. Am. Chem. Soc.* **1994**, *116*, 4461−4462.

(25) Young, M. A.; Ravishanker, G.; Beveridge, D. L. A 5-Nanosecond Molecular Dynamics Trajectory for B-DNA: Analysis of Structure, Motions, and Solvation. *Biophys. J.* **1997**, *73*, 2313−2336.

(26) Cheatham, T. E.; Kollman, P. A. Observation of the A-DNA to B-DNA Transition During Unrestrained Molecular Dynamics in Aqueous Solution. *J. Mol. Biol.* **1996**, *259*, 434−444.

(27) Beveridge, D. L.; Maye, P. V.; Jayaram, B.; Ravishanker, G.; Mezei, M. Aqueous Hydration of Nucleic Acid Constituents: Monte Carlo Computer Simulation Studies. *J. Biomol. Struct. Dyn.* 1984, *2*, 261−270.

(28) Beveridge, D. L.; Swaminathan, S.; Ravishanker, G.; Withka, J. M.; Srinivasan, J.; Prevost, C.; Louise-May, S.; Langley, D. R.; DiCapua, F. M.; Bolton, P. H. Molecular Dynamics Simulations on the Hydration, Structure and Motions of DNA Oligomers. In *Water and Biological Macromolecules*; Westhof, E., Ed.; CRC Press: Boca Raton, FL, 1993; pp 165−225.

(29) Feig, M.; Pettitt, B. M. Crystallographic Water Sites from a Theoretical Perspective. *Structure* **1998**, *6*, 1351−1354.

(30) Feig, M.; Pettitt, B. M. Modeling High-resolution Hydration Patterns in Correlation with DNA Sequence and Conformation. *J. Mol. Biol.* **1999**, *286*, 1075−1095.

(31) Feig, M.; Pettitt, B. M. Sodium and Chlorine Ions as Part of the DNA Solvation Shell. *Biophys. J.* **1999**, *77*, 1769−1781.

(32) Schneider, B.; Cohen, D. M.; Schleifer, L.; Srinivasan, A. R.; Olson, W. K.; Berman, H. M. A Systematic Method for Studying the Spatial Distribution of Water Molecules around Nucleic Acid Bases. *Biophys. J.* **1993**, *65*, 2291−2303.

(33) Schneider, B.; Berman, H. M. Hydration of the DNA Bases is Local. *Biophys. J.* **1995**, *69*, 2661−2669.

(34) Makarov, V.; Pettitt, B. M.; Feig, M. Solvation and hydration of proteins and nucleic acids: A theoretical view of simulation and experiment. *Acc. Chem. Res.* **2002**, *35*, 376−384.

(35) Beveridge, D. L.; McConell, K. J.; Nirmala, R.; Young, M. A.; Vijayakumar, S.; Ravishanker, G. Recent Progress in Molecular Dynamics Simulations of DNA and Protein-DNA Complexes Including Solvent. *ACS Symp. Ser.* **1994**, *568*, 381−394.

(36) Beveridge, D. L.; McConell, K. J.; Nirmala, R.; Young, M. A.; Vijayakumar, S.; Ravishanker, G. Molecular Dynamics Simulations of DNA and a Protein-DNA Complex Including Solvent. In *Modelling of Biomolecular Structures and Mechanisms*; Pullman, A., e.t al., Ed.; Kluwer Acade,oc Publishers: Dordrecht, The Netherlands, 1995; pp 409−423.

(37) Tang, Y.; Nilsson, L. Interaction of Human SRY Protein with DNA: A Molecular Dynamics Study. *Proteins* **1998**, *31*, 417−433.

(38) Tang, Y.; Nilsson, L. Molecular Dynamics Simulations of the Complex between Human U1A Protein and Hairpin II of U1 Small Nuclear RNA and of Free RNA in Solution. *Biophys. J.* **1999**, *77*, 1284−1305.

(39) Kosztin, D.; Bishop, T. C.; Schulten, K. Binding of the Estrogen Receptor on DNA: The Role of Waters. *Biophys. J.* **1997**, *73*, 557−570.

(40) Karplus, M. Molecular dynamics simulations of biomolecules. *Acc. Chem. Res.* **2002**, *35*, 321−323.

(41) Makarov, V. A.; Feig, M.; Pettitt, B. M. Diffusion of Solvent around Biomolecular Solutes. A Molecular Dynamics Simulations Study. *Biophys. J.* **1998**, *75*, 150−158.

(42) Leeuw, S. W. d.; Perram, J. W.; Smith, E. R. Simulation of Electrostatic Systems in Periodic Boundary Conditions. I. Lattice Sums and Dielectric Constants. *Proc. R. Soc., London A* **1980**, *373*, 27−56.

(43) Reed, M. S. C.; Flurchick, K. M. Investigation of Artifacts Due to Periodic Boundary Conditions. *Comput. Phys. Commun.* **1996**, *95*, 39−46.

(44) Roux, B.; Simonson, T. Implicit Solvent Models. *Biophys. Chem.* **1999**, *78*, 1−20.

(45) Honig, B.; Nicholls, A. Classical Electrostatics in Biology and Chemistry. *Science* **1995**, *268*, 1144−1149.

(46) Baker, N.; Holst, M.; Wang, F. Adaptive Multilevel Finite Element Solution of the Poisson−Boltzmann Equation II. Refinement at Solvent-Accessible Surfaces in Biomolecular Systems. *J. Comput. Chem.* **2000**, *21*, 1343−1352.

(47) Boschitsch, A. H.; Fenley, M. O.; Zhou, H.-X. Fast Boundary Element Method for the Linear Poisson−Boltzmann Equation. *J. Phys. Chem. B* **2002**, *106*, 2741−2754.

(48) Holst, M.; Baker, N.; Wang, F. Adaptive Multilevel Finite Element Solution of the Poisson−Boltzmann Equation I. Algorithms and Examples. *J. Comput. Chem.* **2000**, *21*, 1319−1342.

(49) Cortis, C. M.; Friesner, R. A. Numerical Solution of the Poisson−Boltzmann Equation Using Tetrahedral Finite-Element Meshes. *J. Comput. Chem.* **1997**, *18*, 1591−1608.

(50) Warwicker, J.; Watson, H. C. Calculation of the Electric Potential in the Active Site Cleft due to α-Helix Dipoles. *J. Mol. Biol.* **1982**, *157*, 671−679.

(51) Gilson, M. K.; Sharp, K. A.; Honig, B. H. Calculating the Electrostatic Potential of Molecules in Solution: Method and Error Assessment. *J. Comput. Chem.* **1987**, *9*, 327−335.

(52) Prabhu, N. V.; Zhu, P. J.; Sharp, K. A. Implementation and testing of stable, fast implicit solvation in molecular dynamics using the smooth-permittivity finite difference Poisson−Boltzmann method. *J. Comput. Chem.* **2004**, *25* (16), 2049−2064.

(53) Lu, Q.; Luo, R. A Poisson−Boltzmann dynamics method with nonperiodic boundary condition. *J. Chem. Phys.* **2003**, *119* (21), 11035−11047.

(54) Luo, R.; David, L.; Gilson, M. K. Accelerated Poisson−Boltzmann Calculations for Static and Dynamic Systems. *J. Comput. Chem.* **2002**, *23*, 1244−1253.

(55) Im, W.; Beglov, D.; Roux, B. Continuum Solvation Model: Computation of Electrostatic Forces from Numerical Solutions to the Poisson−Boltzmann Equation. *Comput. Phys. Commun.* **1998**, *111*, 59−75.

(56) Bordner, A. J.; Huber, G. A. Boundary Element Solution of the Linear Poisson−Boltzmann Equation and a Multipole Method for the Rapid Calculation of Forces on Macromolecules in Solution. *J. Comput. Chem.* **2003**, *24*, 353−367.

(57) Friedrichs, M.; Zhou, R. H.; Edinger, S. R.; Friesner, R. A. Poisson−Boltzmann analytical gradients for molecular modeling calculations. *J. Phys. Chem. B* **1999**, *103*, 3057−3061.

(58) Sharp, K. Incorporating Solvent and Ion Screening into Molecular Dynamics Using the Finite-Difference Poisson−Boltzmann Method. *J. Comput. Chem.* **1991**, *12*, 454−468.

(59) Fan, H.; Mark, A. E.; Zhu, J.; Honig, B. Comparative study of generalized Born models: Protein dynamics. *Proc. Natl. Acad. Sci. U.S.A.* **2005**, *102* (19), 6760−6764.

(60) Lee, M. S.; Feig, M.; Salsbury, F. R., Jr.; Brooks, C. L., III New Analytical Approximation to the Standard Molecular Volume Definition And Its Application to Generalized Born Calculations. *J. Comput. Chem.* **2003**, *24*, 1348−1356.

(61) Feig, M.; Onufriev, A.; Lee, M. S.; Im, W.; Case, D. A.; Brooks, C. L., III Performance Comparison of Generalized Born and Poisson Methods in the Calculation of Electrostatic Solvation Energies for Protein Structures. *J. Comput. Chem.* **2004**, *25*, 265−284.

(62) Im, W.; Lee, M. S.; Brooks, C. L., III Generalized Born model with a simple smoothing function. *J. Comput. Chem.* **2003**, *24*, 1691−1702.

(63) Ghosh, A.; Rapp, C. S.; Friesner, R. A. Generalized Born Model Based on a Surface Integral Formulation. *J. Phys. Chem. B* **1998**, *102*, 10983−10990.

(64) Still, W. C.; Tempczyk, A.; Hawley, R. C.; Hendrickson, T. Semianalytical Treatment of Solvation for Molecular Mechanics and Dynamics. *J. Am. Chem. Soc.* **1990**, *112*, 6127−6129.

(65) Qiu, D.; Shenkin, P. S.; Hollinger, F. P.; Still, W. C. The GB/SA Continuum Model for Solvation. A Fast Analytical Method for the Calculation of Approximate Born Radii. *J. Phys. Chem. A* **1997**, *101*, 3005−3014.

(66) Feig, M.; Brooks, C. L., III Recent advances in the development and application of implicit solvent models in biomolecule simulations. *Curr. Opin. Struct. Biol.* **2004**, *14*, 217−224.

(67) Hawkins, G.; Cramer, C.; Truhlar, D. Pairwise descreening of solute charges from a dielectric medium. *Chem. Phys. Lett.* **1995**, *246*, 122−129.

(68) Onufriev, A.; Case, D. A.; Bashford, D. Effective Born Radii in the Generalized Born Approximation: The Importance of Being Perfect. *J. Comput. Chem.* **2002**, *23*, 1297−1304.

(69) Scarsi, M.; Apostolakis, J.; Caflisch, A. Continuum electrostatic energies of macromolecules in aqueous solutions. *J. Phys. Chem. A* **1997**, *101* (43), 8098−8106.

(70) Bashford, D.; Case, D. A. Generalized Born models of macromolecular solvation effects. *Annu. Rev. Phys. Chem.* **2000**, *51*, 129−152.

(71) Schaefer, M.; Froemmel, C. A Precise Analytical Method for Calculating the Electrostatic Energy of Macromolecules in Aqueous-Solution. *J Mol. Biol.* **1990**, *216* (4), 1045−1066.

(72) Dominy, B. N.; Brooks, C. L., III Development of a Generalized Born Model Parametrization for Proteins and Nucleic Acids. *J. Phys. Chem. B* **1999**, *103*, 3765−3773.

(73) Lee, M. S.; Salsbury, F. R., Jr.; Brooks, C. L., III, Novel generalized Born methods. *J. Chem. Phys.* **2002**, *116* (24), 10606−10614.

(74) Lee, B.; Richards, F. M. Interpretation of Protein Structures—Estimation of Static Accessibility. *J. Mol. Biol.* **1971**, *55*, 379.

(75) Richards, F. M. Areas, Volumes, Packing, and Protein-Structure *Annu. Rev. Biophys. Bioeng.* **1977**, *6*, 151−176.

(76) Nina, M.; Beglov, D.; Roux, B. Atomic Radii for Continuum Electrostatics Calculations Based on Molecular Dynamics Free Energy Simulations. *J. Phys. Chem.* **1997**, *101*, 5239−5248.

(77) Sitkoff, D.; Sharp, K. A.; Honig, B. Accurate Calculation of Hydration Free-Energies Using Macroscopic Solvent Models. *J. Phys. Chem.* **1994**, *98*, 1978−1988.

(78) Zhu, J.; Shi, Y.; Liu, H. Parametrization of a Generalized Born/Solvent-Accessible Surface Area Model and Applications to the Simulation of Protein Dynamics. *J. Phys. Chem. B* **2002**, *106*, 4844−4853.

(79) Swanson, J. M. J.; Adcock, S. A.; McCammon, J. A. Optimized radii for Poisson−Boltzmann calculations with the AMBER force field. *J. Chem. Theory Comput.* **2005**, *1* (3), 484−493.

(80) Geney, R.; Layten, M.; Gomperts, R.; Hornak, V.; Simmerling, C. Investigation of salt bridge stability in a generalized born solvent model. *J. Chem. Theory Comput.* **2006**, *2* (1), 115−127.

(81) Banavali, N. K.; Roux, B. Atomic Radii for Continuum Electrostatics Calculations on Nucleic Acids. *J. Phys. Chem. B* **2002**, *106*, 11026−11035.

(82) Rapp, C. S.; Friesner, R. A. Prediction of Loop Geometries Using a Generalized Born Model of Solvation Effects. *Proteins* **1999**, *35*, 173−183.

(83) Calimet, N.; Schaefer, M.; Simonson, T. Protein Molecular Dynamics With the Generalized Born/ACE Solvent Model. *Proteins* **2001**, *45*, 144−158.

(84) David, L.; Luo, R.; Gilson, M. K. Comparison of Generalized Born and Poisson Models: Energetics and Dynamics of HIV Protease. *J. Comput. Chem.* **2000**, *21*, 295−309.

(85) Gallicchio, E.; Zhang, L. Y.; Levy, R. M. The SGB/NP Hydration Free Energy Model Based on the Surface Generalized Born Solvent Reaction Field and Novel Nonpolar Hydration Free Energy Estimators. *J. Comput. Chem.* **2002**, *23*, 517−529.

(86) Liu, Y.; Beveridge, D. L. Exploratory Studies of Ab Initio Protein Structure Prediction: Multiple Copy Simulated Annealing AMBER Energy Functions, and a Generalized Born/Solvent Accessibility Solvation Model. *Proteins* **2002**, *46*, 128−146.

(87) Xia, B.; Tsui, V.; Case, D. A.; Dyson, H. J.; Wright, P. E. Comparison of protein solution structures refined by molecular dynamics simulation in a vacuum, with a generalized Born model, and with explicit water. *J. Biomol. NMR* **2002**, *22*, 317−331.

(88) Zhang, L. Y.; Gallicchio, E.; Friesner, R. A.; Levy, R. M. Solvent Models for Protein-Ligand Binding: Comparison of Implicit Solvent Poisson and Surface Generalized Born Models with Explicit Solvent Simulations. *J. Comput. Chem.* **2001**, *22*, 591−607.

(89) Tsui, V.; Case, D. A. Theory and Applications of the Generalized Born Solvation Model in Macromolecular Simulations. *Biopolymers* (*Nucleic Acid Sci.*) **2001**, *56*, 275−291.

(90) Felts, A. K.; Gallicchio, E.; Wallqvist, A.; Levy, R. M. Distinguishing Native Conformations of Proteins From Decoys With an Effective Free Energy Estimator Based on the OPLS All-Atom Force Field and the Surface Generalized Born Solvent Model. *Proteins* **2002**, *48*, 404−422.

(91) Nymeyer, H.; Garcia, A. E. Simulation of the folding equilibrium of α-helical peptides: A comparison of the generalized Born approximation with explicit solvent. *Proc. Natl. Aacd. Sci. U.S.A.* **2003**, *100*, 13934−13939.

(92) Bursulaya, B. D.; Brooks, C. L., III Comparative Study of the Folding Free Energy Landscape of a Three-Stranded β-Sheet Protein with Explicit and Implicit Solvent Models. *J. Phys. Chem. B* **2000**, *104* (51), 12378−12383.

(93) Tanizaki, S.; Feig, M. A generalized Born formalism for heterogeneous dielectric environments: Application to the implicit modeling of biological membranes. *J. Chem. Phys.* **2005**, *122*, 124706.

(94) Scarsi, M.; Apostolakis, J.; Caflisch, A. Comparison of a GB solvation model with explicit solvent simulations: Potentials of mean force and conformational preferences of alanine dipeptide and 1,2-dichloroethane. *J. Phys. Chem. B* **1998**, *102* (18), 3637−3641.

(95) Tsui, V.; Case, D. A. Molecular dynamics simulations of nucleic acids with a generalized Born solvation model. *J. Am. Chem. Soc.* **2000**, *122*, 2489−2498.

(96) Wang, L.; HIngerty, B. E.; Srinivasan, A. R.; Olson, W. K.; Broyde, S. Accurate Representation of B-DNA Double Helical Structure with Implicit Solvent and Counterions. *Biophys. J.* **2002**, *83*, 382−406.

(97) Srinivasan, J.; Cheatham, T. E.; Cieplak, P.; Kollman, P. A.; Case, D. A. Continuum Solvent Studies of the Stability of DNA, RNA, and Phosphoramidate-DNA Helices. *J. Am. Chem. Soc.* **1998**, *120*, 9401−9409.

(98) Zacharias, M.; Sklenar, H. Analysis of the Stability of Looped-Out and Stacked-In Conformations of an Adenine Bulge in DNA Using a Continuum Model for Solvent and Ions. *Biophys. J.* **1997**, *73*, 2990−3003.

(99) Denisov, V. P.; Carlstrom, G.; Halle, B. Kinetics of DNA Hydration. *J. Mol. Biol.* **1997**, *268*, 118−136.

(100) Forsyth, V. T.; Mahendrasingam, A.; Pigram, W. J.; Greenall, R. J.; Bellamy, K.; Fuller, W.; Mason, S. A. Neutron Fibre Diffraction Study of DNA Hydration. *Int. J. Biol. Macromol.* **1989**, *11*, 236−240.

(101) Poltev, V. I.; Malenkov, G. G.; Gonzalez, E. J.; Teplukhin, A. V.; Rein, R.; Shibata, M.; Miller, J. H. Modeling DNA Hydration: Comparison of Calculated and Experimental Hydration Properties of Nucleic Acid Bases. *J. Biomol. Struct. Dyn.* **1996**, *13*, 717−725.

(102) Tao, N. J.; Linsway, S. M.; Rupprecht, A. Structure of DNA Hydration Shells Studied by Raman Spectroscopy. *Biopolymers* **1989**, *28*, 1019−1030.

(103) Chalikian, T. V.; Völker, J.; Srinivasan, A. R.; Olson, W. K.; Breslauer, K. J. The Hydration of Nucleic Acid Duplexes as Assessed by a Combination of Volumetric and Structural Techniques. *Biopolymers* **1999**, *50*, 459−471.

(104) Ewald, P. P. Die Berechnung optischer und elektrostatischer Gitterpotentiale. *Ann. Phys.* **1921**, *64*, 253−287.

(105) Sagui, C.; Darden, T. A. Molecular dynamics simulations of biomolecules: Long-range electrostatic effects. *Annu. Rev. Biophys. Biomol. Struct.* **1999**, *28*, 155−179.

(106) Cheatham, T. E.; Miller, J. L.; Fox, T.; Darden, T. A.; Kollman, P. A. Molecular Dynamics Simulations on Solvated Biomolecular Systems: The Particle Mesh Ewald Method Leads to Stable Trajectories of DNA, RNA, and Proteins. *J. Am. Chem. Soc.* **1995**, *117*, 4193−4194.

(107) Norberg, J.; Nilsson, L. On the truncation of long-range electrostatic interactions in DNA. *Biophys. J.* **2000**, *79* (3), 1537−1553.

(108) Shui, X.; McFail-Isom, L.; Hu, G. G.; Williams, L. D. The B-DNA Dodecamer at High Resolution Reveals a Spine of Water on Sodium. *Biochemistry* **1998**, *37*, 8341−8355.

(109) Denisov, V. P.; Halle, B. Sequence-specific binding of counterions to B-DNA. *Proc. Natl. Acad. Sci. U.S.A.* **2000**, *97* (2), 629−633.

(110) Anderson, C. F.; Record, M. T. Ion distributions around DNA and other cylindrical polyions: theoretical descriptions and physical implications. *Annu. Revi. Biophys. Biophys. Chem.* **1990**, *19*, 423−465.

(111) Manning, G. S. The Molecular Theory of Polyelectrolyte Solutions with Applications to the Electrostatic Properties of Polynucleotides. *Q. Rev. Biophys.* **1978**, *11*, 179−246.

(112) Young, M. A.; Jayaram, B.; Beveridge, D. L. Intrusion of Counterions into the Spine of Hydration in the Minor Groove of B-DNA: Fractional Occupancy of Electronegative Pockets. *J. Am. Chem. Soc.* **1997**, *119*, 59−69.

(113) Ponomarev, S. Y.; Thayer, K. M.; Beveridge, D. L. Ion motions in molecular dynamics simulations on DNA. *Proc. Natl. Acad. Sci. U.S.A.* **2004**, *101* (41), 14771−14775.

(114) Cheatham, T. E.; Young, M. A. Molecular dynamics simulation of nucleic acids: Successes, limitations, and promise. *Biopolymers* **2000**, *56* (4), 232−256.

(115) Nishimura, Y.; Torigoe, C.; Tsuboi, M. Salt Induced B−A Transition of Poly(dG)·Poly(dC) and the Stabilization of A Form by its Methylation. *Nucleic Acids Res.* **1986**, *14*, 2737−2748.

(116) Drew, H. R.; Wing, R. M.; Takano, T.; Broka, C.; Tanaka, S.; Itakura, K.; Dickerson, R. E. Structure of a B-DNA Dodecamer: Conformation and Dynamics. *Proc. Natl. Acad. Sci. U.S.A.* **1981**, *78*, 2179−2183.

(117) Drew, H. R.; Dickerson, R. E. Structure of a B-DNA Dodecamer. III. Geometry of Hydration. *J. Mol. Biol.* **1981**, *151*, 535−556.

(118) MacKerell, A. D., Jr.; Banavali, N. K. All-Atom Empirical Force Field for Nucleic Acids: II. Application to Molecular Dynamics Simulations of DNA and RNA in Solution. *J. Comput. Chem.* **2000**, *21*, 105−120.

(119) Allen, M. D.; Yamasaki, K.; Ohme-Takagi, M.; Tateno, M.; Suzuki, M. A novel mode of DNA recognition by a beta-sheet revealed by the solution structure of the GCC-box binding domain in complex with DNA. *Embo J.* **1998**, *17* (18), 5484−5496.

(120) Foloppe, N.; MacKerell, A. D., Jr. All-Atom Empirical Force Field for Nucleic Acids: I. Parameter Optimization Based on Small Molecule and Condensed Phase Macromolecular Target Data. *J. Comput. Chem.* **2000**, *21*, 86−104.

(121) MacKerell, A. D., Jr.; Bashford, D.; Bellott, M.; Dunbrack, J. D.; Evanseck, M. J.; Field, M. J.; Fischer, S.; Gao, J.; Guo, H.; Ha, S.; Joseph-McCarthy, D.; Kuchnir, L.; Kuczera, K.; Lau, F. T. K.; Mattos, C.; Michnick, S.; Ngo, T.; Nguyen, D. T.; Prodhom, B.; Reiher, W. E.; Roux, B.; Schlenkrich, M.; Smith, J. C.; Stote, R.; Straub, J.; Watanabe, M.; Wiorkiewicz-Kuczera, J.; Yin, D.; Karplus, M. All-Atom Empirical Potential for Molecular Modeling and Dynamics Studies of Proteins. *J. Phys. Chem. B* **1998**, *102*, 3586−3616.

(122) MacKerell, A. D., Jr.; Feig, M.; Brooks, C. L., III Extending the treatment of backbone energetics in protein force fields: Limitations of gas-phase quantum mechanics in reproducing protein conformational distributions in molecular dynamics simulations. *J. Comput. Chem.* **2004**, *25*, 1400−1415.

(123) MacKerell, A. D., Jr.; Feig, M.; Brooks, C. L., III Improved treatment of the protein backbone in empirical force fields. *J. Am. Chem. Soc.* **2004**, *126*, 698−699.

(124) Chocholousova, J.; Feig, M. Balancing an Accurate Representation of the Molecular Surface in Generalized Born Formalisms with Integrator Stability in Molecular Dynamics Simulations. *J. Comput. Chem.* **2006**, *27*, 719−729.

(125) Srinivasan, J.; Trevathan, M. W.; Beroza, P.; Case, D. A. Application of a pairwise generalized Born model to proteins and nucleic acids: Inclusion of salt effects. *Theor. Chim. Acta* **1999**, 101, 426−434.

(126) Tjandra, N.; Tate, S.; Ono, A.; Kainosho, M.; Bax, A. The NMR structure of a DNA dodecamer in an aqueous dilute liquid crystalline phase. *J. Am. Chem. Soc.* **2000**, *122* (26), 6190−6200.

(127) Lu, X. J.; Olson, W. K. 3DNA: a software package for the analysis, rebuilding and visualization of three-dimensional nucleic acid structures. *Nucleic Acids Res.* **2003**, *31* (17), 5108−5121.

(128) Pastor, R. W.; Brooks, B. R.; Szabo, A. An Analysis of the Accuracy of Langevin and Molecular-Dynamics Algorithms. *Mol. Phys.* **1988**, *65* (6), 1409−1419.

(129) Brooks, B. R.; Bruccoleri, R. E.; Olafson, B. D.; States, D. J.; Swaminathan, S.; Karplus, M. CHARMM: A Program for Macromolecular Energy, Minimization, and Dynamics Calculations. *J. Comput. Chem.* **1983**, *4*, 187−217.

(130) Feig, M.; Karanicolas, J.; Brooks, C. L., III MMTSB Tool Set: Enhanced Sampling and Multiscale Modeling Methods for Applications in Structural Biology. *J. Mol. Graph. Model.* **2004**, *22*, 377−395.

(131) Cheatham, T. E., III: ptraj − analysis module of AMBER.
(132) Dickerson, R. E. DNA Bending: The Prevalence of Kinkiness and the Virtues of Normality. *Nucleic Acids Res.* **1998**, *26*, 1906−1926.
(133) MacKerell, A. D., Jr.; Banavali, N. K. All-Atom Empirical Force Field for Nucleic Acids: II. Application to Molecular Dynamics Simulations of DNA and RNA in Solution. *J. Comput. Chem.* **2000**, *21*, 105−120.
(134) Kopka, M. L.; Fratini, A. V.; Drew, H. R.; Dickerson, R. E. Ordered Water Structure Around a B-DNA Dodecamer. A Quantitative Study. *J. Mol. Biol.* **1983**, *163*, 129−146.
(135) Giudice, E.; Varnai, P.; Lavery, R. Base pair opening within B-DNA: Free energy pathways for GC and AT pairs from umbrella sampling simulations. *Nucleic Acids Res.* **2003**, *31*, 1434−1443.
(136) Pan, Y. P.; MacKerell, A. D. Altered structural fluctuations in duplex RNA versus DNA: a conformational switch involving base pair opening. *Nucleic Acids Res.* **2003**, *31* (24), 7131−7140.
(137) Pan, Y. P.; MacKerell, A. A conformational switch involving local base pair opening in duplex RNA. *Biophys. J.* **2004**, *86* (1), 145A−145A.
(138) van Aalten, D. M. F.; Erlanson, D. A.; Verdine, G. L.; Joshua-Tor, L. A structural snapshot of base-pair opening in DNA. *Proc. Natl. Acad. Sci. U.S.A.* **1999**, *96* (21), 11809−11814.
(139) Dornberger, U.; Leijon, M.; Fritzsche, H. High base pair opening rates in tracts of GC base pairs. *J. Biol. Chem.* **1999**, *274* (11), 6957−6962.
(140) Wang, Y.; Thomas, G. A.; Peticolas, W. L. A Duplex of the Oligonucleotides d(GGGGGTTTTT) and d(AAAAACCCCC) Forms an A to B Conformational Junction in Concentrated Salt Solutions. *J. Biomol. Struct. Dyn.* **1989**, *6*, 1177−1187.
(141) Cheatham, T. E.; Crowley, M. F.; Fox, T.; Kollman, P. A. A Molecular Level Picture of the Stabilization of A-DNA in Mixed Ethanol−Water Solutions. *Proc. Natl. Acad. Sci. U.S.A.* **1997**, *94*, 9626−9630.
(142) Cheatham, T. E.; Kollman, P. A. Insight into the Stabilization of A-DNA by Specific Ion Association: Spontaneous B-DNA to A-DNA Transitions Observed in Molecular Dynamics Simulations of d(ACCC-GCGGGT)$_2$ in the Presence of Hexaamminecobalt(III). *Structure* **1997**, *15*, 1297−1311.
(143) Wahl, M. C.; Sundaralingam, M. Crystal Structures of A-DNA Duplexes. *Biopolymers* (*Nucleic Acid Sci.*) **1997**, *44*, 45−63.
(144) Debye, P.; Huckel, E. The theory of electrolytes I. The lowering of the freezing point and related occurrences. *Phys. Z.* **1923**, *24*, 185−206.
(145) Debye, P.; Huckel, E. The theory of the electrolyte II−The border law for electrical conductivity. *Phys. Z.* **1923**, *24*, 305−325.
(146) Baucom, J.; Transue, T.; Fuentes-Cabrera, M.; Krahn, J. M.; Darden, T. A.; Sagui, C. Molecular dynamics simulations of the d(CCA-ACGTTGG)(2) decamer in crystal environment: Comparison of atomic point-charge, extra-point, and polarizable force fields. *J. Chem. Phys.* **2004**, *121* (14), 6998−7008.